NUMERICAL MODELING OF HYDRAULIC FRACTURE PROPAGATION USING FEA IN SHALE RESERVOIRS

Pablo A. Medina[1], Marcelo Frydman[2], Joaquin Eiff[1], Maria Moine[1], Juan Mujica[1], Sebastian D'hers[1]

[1]*Computational Mechanics Center, Mechanical Engineering Dept. Instituto Tecnológico de Buenos Aires.*
Av. Madero 399, ZC1106, Buenos Aires/CABA, Argentina
pmedina@itba.edu.ar, jeiff@itba.edu.ar, mmoine@itba.edu.ar, sdhers@itba.edu.ar
[2]*Geomechanics advisor*
Buenos Aires/CABA, Argentina
mfrydman2@outlook.com

Abstract. The aim of fracking procedures is enhancing the permeability of non-conventional reservoirs. This process is influenced by the in-situ stresses. Throughout history, in Vaca Muerta (Argentina), wells production has been technically challenging. Vaca Muerta formation is made of shale and limestone layers which induce a difference in the in-situ stresses. In a strike-slip regime this stress difference in combination with the geomechanical properties might promote the appearance of horizontal fractures. Given the above, the following research discusses numerical modeling of the stresses during the fracking procedure.

Several numerical experiments will be presented to identify opportunities to optimize operations in Vaca Muerta, considering different features, such as: geomechanical properties, weak interfaces (density and properties), and laminations (shale vs limestone).

This work presents numerical results concerning the growth of a vertical hydraulic fracture in a 3D shale domain. This fracture growth is limited by a thin layer of limestone, which creates a weak interface between the limestone and shale. The goal of this analysis is focused on the interaction mechanism between the weak interface and the growth of the vertical fracture. Arrest, crossing and T-shapes fractures can take place. A cohesive mode with mixed damage is carried out. Furthermore, this study explores different properties for the limestone layer, given by a geomechanical model from Vaca Muerta, effect in fracture growth. Results will provide an optimized operating window for injection and fracture process in order to improve the resultant stimulated reservoir volume.

Keywords: Fracking, Weak interface, T-shape fractures, dilatancy.

1 Introduction

The aim of fracking technique is to propagate fractures only confined by the producible reservoir zones. In a laminated formation such as Vaca Muerta, Argentina, weak interfaces (WI) are commonly found between intercalations of organic shale with limestone. Both shale and limestone, in addition to other formations, have transversely isotropic properties. This property occurs in the axes contained in the bedding plane. Said description of properties arise from the formation process of each layer, as stated by Sosa and Frydman [1]. As a consequence, the in-situ stresses variations and rock properties are of more importance than the horizontal variations. The above mentioned WI alters the hydraulic fracture growth, giving different types of interaction mechanisms, as stated by Blanton [2]. The WI plane acts as a barrier for the height growth, in line with Celleri [3]. This phenomena can promote t-shape fractures, which will reduce the stimulated hydraulic fracture area. As a consequence, the fracturing process will not be optimal.

Most geomechanical models used by the industry are analytical solutions based on simple assumptions. The early well known works in the area of hydraulic fracture modeling were proposed by Khristianovic and Zheltov [4] and Perkins and Kern [5]. These models assume a planar geometry for the fracture. One step forward in modeling this problem under more realistic conditions is given by Adachi [6] and Weng [7]. However, the utility of these analytical solutions are restricted by several hypothesis and their application must be done carefully. To deal with

the complexity of the problem, numerical models are the key to address a more realistic solution. Some of them were proposed by different authors: Nguyen [8], Serebrinsky [9], Frydman [10].

Nowadays, most fracking simulators ignore the interaction between the hydraulic fracture and the WI, giving as a result an overestimation of the fracture height compared to field observations, as stated by Daneshy [11]. Analytical model to represent this mechanism were proposed by Chuprakov [12].

This paper presents a numerical model using the Biot's poroelastic theory, published by Detournay [13]. Non-linear fracture propagation model (interface elements) is carried out, as stated by de Borst [14] and its an extension from the implemented approach by Medina et al [15]. The analysis is focused on the different parameters which affect in the interaction between an hydraulic fracture propagation and a WI plane. The dilatancy angle and mechanical properties for the limestone barrier will be studied. Different scenarios are modeled and a sensitive analysis is performed to provide an optimized operating window to improve stimulated area.

2 Governing equation for the model

In order to take into account the physics of the problem, we divide this in 4 stages, which are: fracture initiation, fluid flow into the fracture, seepage into the porous media (leak off) and the mechanical deformation of the porous media. The poroelastic media can be represented by two domains, the hydraulic fracture zone Γ_d and the porous media Ω. In poroelastic media, the mechanical deformation is followed by an adjustment in pore pressure due to the seepage of the pore fluid between the pores. The fluid flow between pores is described by the Darcy flow law and is dictated by the permeability of the formation. Because of strong nonlinear coupling between these processes, obtaining a mathematical solution requires solving a nonlinear system. This system includes the equations of poroelasticity governing matrix deformation and the associated fluid diffusion in the porous media. Biot's theory is adopted to model the porous media, as stated by Detournay [13] and a cohesive model with mixed damage (mode I and mode II) is implemented to describe the fracture behaviour, in agreement with Scheider [16]. The governing equations of each physical processes are summarized in Medina et al [15].

Dilatancy

In a recent work, Medina et al [15] proposed the expression given by eq. (1) to take into account the dilatancy effects on the permeability in the weak interface plane between shale and limestone formation.

$$h = [[u]]_n + tan\psi\sqrt{[[u]]^2_{s-1} + [[u]]^2_{s-2}}. \tag{1}$$

Where h is the fracture aperture in the Poiseuille flow equation, $[[u]]_n$ is the normal relative displacement between parallel plates, $[[u]]^2_{s-1}$ and $[[u]]^2_{s-2}$ are the tangential relative displacements in both directions and ψ is the dilatancy angle in the weak interface. In order to satisfy equation (1) several hypotheses are taken into account. The dilatancy angle is restricted to the fracture plane, and therefore does not represent the change in volume associated with the shear distortion of an element in the material. Moreover, eq. (1) is only valid for small displacements and small strains. However, this expression can be used to address the t-shape fractures in strike fault regimes and its impact during the fracture process.

3 Weak forms equations and discretization

In this section, the weak form of the governing equations are presented. Furthermore, the matricial form of these are introduced. The algebra to arrive at the matrix expression is detailed in Medina et al [15].

3.1 Weak forms of porous domain equations

The weak form of the momentum equation, which was described in the previous work (Medina et al [15]), is obtained by applying the principle of virtual displacements and integrating over the volume Ω.

Linear elements are used to model the poroelastic material (H8 eight nodes hexahedron). The fracture and weak interface are represented by 8-nodes cohesive elements, as stated by de Borst [14]. After some algebra manipulation the final matrix form for bulk domain (Ω) is given by:

$$[K]\{d\}_m - [C_g]\{p\}_m + \{F\}_m = 0. \tag{2}$$

Where d and p are the nodal displacements and the pore pressure field in the bulk domain, respectively.

- $[K] = \int B^T C B \; d\Omega$ is the stiffness matrix ; $[C_g] = \int B^T \alpha m N_p \; d\Omega$ is the coupling matrix ; $\{F\} = \int N^T N q_i \; d\Gamma_t + \int N^T N f_i \; d\Omega + \int B^T \sigma_0^{'} \; d\Omega$ are the traction forces, volume loads and in-situ stresses.

The external load applied to the porous domain is in equilibrium with the effective stresses in the soil phase and the pore pressure of the fluid. Therefore, the effective component of the in-situ stresses can be applied as volume loads coming from residual stresses. Variables $\sigma_0^{'}$ and $\alpha \; p_{p0}$ are the effective stresses and pore pressure field at the beginning of the process ($t = 0$). As stated above, Biot's theory is implemented to represent the porous media behaviour. Two domains can be identified, bulk domain (Ω) and fracture domain (Γ_d). The displacement and pressure fields which correspond to Ω domain will have subindexes "m" and "p", respectively (d_m , p_p). Whereas, the displacements and pressure which correspond to Γ_d domain will have subindexes "i" and "f" (d_i , p_f), respectively. Analogously, after standard manipulations the matrix form for the fracture domain (Γ_d) is given by:

$$[K]\{d\}_i - [C_g]\{p\}_f + \{F\}_i + \{F_c\} - [K_{coh}]\{d\}_i - [M_j]\{p\}_f = 0. \tag{3}$$

Where:

- $\{F_c\} = \int N_i^T \sigma_0 \; d\Gamma_d + \int N_i^T K_e [[u]]_0 \; d\Gamma_d$ is the internal cohesive force ; $[K_{coh}] = \int N_i^T K_e [[u]] \; d\Gamma_d$ is the cohesive stiffness matrix ; $[M_j] = \int N_i^T \alpha_f m N_f p_f \; d\Gamma_d$ is the coupling matrix for the cohesive element.

Accordingly, the weak form of the pore fluid diffusion equation is obtained applying the virtual power principle to the conservation equation. The matrix form for the bulk domain (Ω) can be written as:

$$[C_g]^T \{\frac{\partial d}{\partial t}\}_m + [S]\{\frac{\partial p}{\partial t}\}_p + [K_p]\{p\}_p - \{q\}_p = 0. \tag{4}$$

Where:

- $[S] = \int N_p^T S N_p \; d\Omega$ is the storativity matrix ; $[K_g] = \int \nabla N_p^T (\frac{\kappa}{\mu}) \nabla N_p p_p \; d\Omega$ is the permeability matrix ; $\{q\}_p = \int N_p^T q_n \; d\Gamma_d$ is a source term.

3.2 Weak form of the fracturing fluid equation

As in pore fluid diffusion equation, the virtual power principle is applied. The matrix form for the fracture domain (Ω) obtained is:

$$[M_j]^T \{\frac{\partial d}{\partial t}\}_i + [S_f]\{\frac{\partial p}{\partial t}\}_f + [H]\{p\}_f + [C_g]^T \{\frac{\partial d}{\partial t}\}_i + [S]\{\frac{\partial p}{\partial t}\}_f + [K_p]\{p\}_f = \{Q\}_f + \{q\}_f. \tag{5}$$

Where: $[K_p] = \int \nabla N_p^T (\frac{h^3}{12\mu}) \nabla N_p p_p \; d\Omega$ is the permeability matrix and h is the fracture aperture given by eq. (1). Details may be found in Medina et al [15].

3.3 Coupling poroelastic system

With the purpose of coupling the poroelastic and fracture domain, a few assumptions will be taken. The fracture opening is tied to fracture height in the eq. (1), and the pore and fracture fluid pressure are considered equal in the fracture bounds. The resulting system of equations to be resolved is given by eqs. (2), (3), (4) and

(5). As the transient terms are discretised using a fully implicit scheme, the system of equations is solved for time t+1. In order to linearize the non-linear terms (e.g. cohesive stiffness matrix), a Newton-Raphson method is proposed. By solving this set of equations altogether, the displacements, pore pressure and fracturing fluid pressure are calculated at once. The in-house developed code allows to capture the strong coupling between the porous medium and the growing fracture.

4 Results

In the current section, the FEA model equations described above are implemented to study the hydraulic fracture propagation. Several geomechanical cases will be presented for performing sensitive analysis. These examples will consider the effect of intercalations of organic shale with limestone barriers and ash beds. The ash beds will be modeled as weak interface between limestone and shale. In each case, the limestone mechanical properties and dilatancy will vary. Dilatancy angle will change from $0°$ up to $30°$. Shale properties are presented in Table 1 and barrier properties for each case are presented in Table 2. Geomechanical data is included in Table 1 and Table 2. These properties are consistent with the ones published by Frydman et al. [17], Varela and Hasbani [18] and Sosa Massaro [19]. Before discussing the results, some definitions must be clarified. The vertical fracture is named the primary fracture, while the horizontal fracture, is the secondary fracture. These are indicated in Fig. 1 where the implemented finite element mesh is illustrated. In addition, each simulation with variations on the physical properties of the layers are called cases and those executed within each case with variations on the dilatancy angle are called sub-cases.

Table 1. Shale properties in Vaca Muerta

Lithology	Depth [m]	Ev [Mpsi]	Eh [Mpsi]	ν_V	ν_H	P_p [psi/ft]	S_v [psi/ft]	S_h [psi/ft]	S_H [psi/ft]
Shale	2953	1.92	2.78	0.23	0.28	0.88	1.04	0.97	1.09

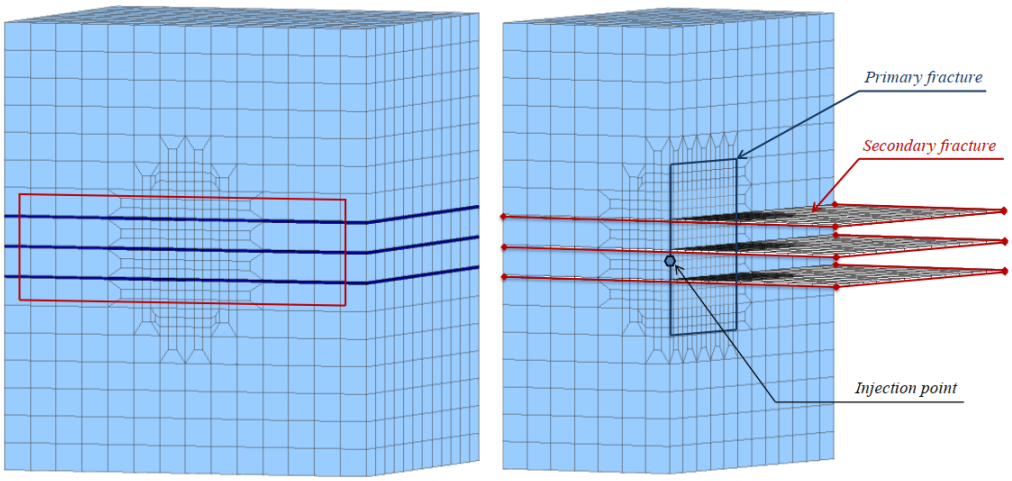

Figure 1. Left: Full domain mesh with limestone barriers. Right: Cross section with the weak interface planes.

The injection point is illustrated in Fig. 1. Homogeneous net pressure is considered with an injection rate of 9 bpm. The rheological properties of the fluid fracture remain constant during all the fracking process.

Table 2. Barriers properties.

Case	Lithology	Depth [m]	Ev [Mpsi]	Eh [Mpsi]	ν_V	ν_H	P_p [psi/ft]	S_v [psi/ft]	S_h [psi/ft]	S_H [psi/ft]
0	Homogeneous Shale	2953	1.92	2.78	0.23	0.28	0.88	1.04	0.97	1.09
1	Clay	2953	1.09	1.57	0.25	0.28	0.88	1.04	0.80	0.87
2	Soft Limestone	2953	2.36	3.04	0.2	0.31	0.88	1.04	0.98	1.13
3	Limestone	2953	3.25	4.98	0.275	0.31	0.88	1.04	1.087	1.28
4	Limestone	2953	3.55	5.25	0.3	0.31	0.88	1.04	1.11	1.31
5	Limestone	2953	3.84	5.51	0.31	0.31	0.88	1.04	1.12	1.33

In Fig. 2 the stress gradients are represented. Due to mechanical properties, it can be seen that where there are more stiff barriers, there are greater horizontal stresses. Because of the difference in limestone properties for each case, an strong contrast between horizontal stresses can be noticed.

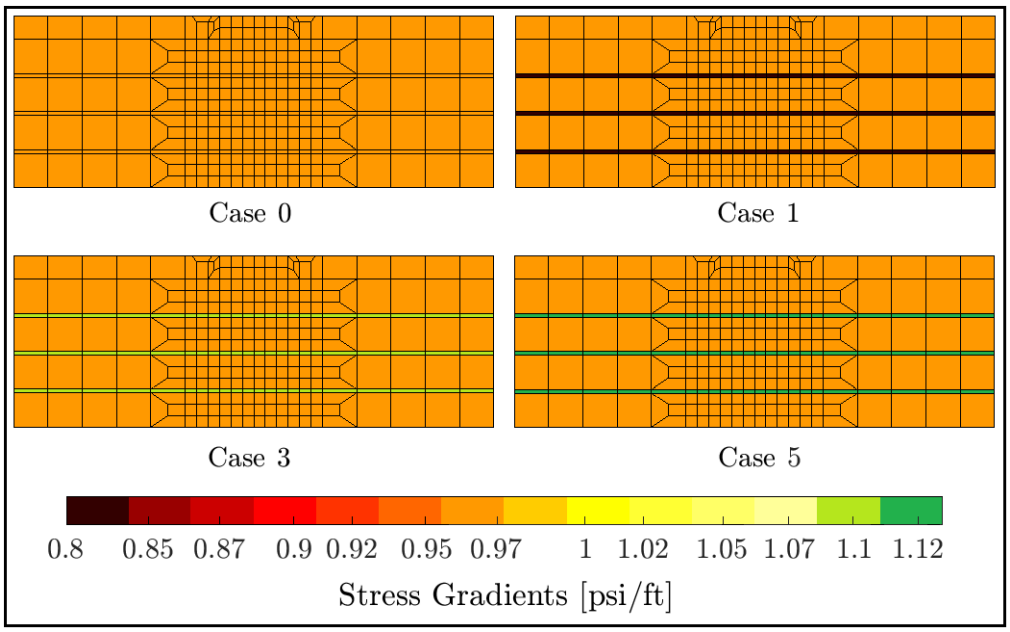

Figure 2. Stress gradients (S_h) for cases of Table 2 (Detail of Fig. 1).

Barrier properties are taken from Hiroki Sone and Mark D. Zoback [20]. Each layer has two meters of thickness. Due to complexity in obtaining the WI properties, some of them are proposed in Table 3.

Table 3. Mechanical properties assumed for the weak interface.

Formation	UCS_v [psi]	TSTR [psi]	E [Mpsi]	ν	Dilatancy Angle
WI	2000	200	0.96	0.23	$0° - 30°$

Where UCS_v and TSTR are the unconfined compressive strength and the tensile strength, respectively.

Note from Table 3 that the dilatancy angle varies between $0°$ and $30°$, the number of sub-cases depends on how redundant they are. It will be seen later that depending on the combinations of properties between layers (see Table 1 and Table 2), the effect of the dilatancy angle is more noticeable when contrast between properties grow. The maximum value ($30°$) is bounded by the internal friction angle, which although is quite high for a dense rock, it is representative to accentuate the results.

4.1 Mechanical properties sensitivity.

In Fig. 4 the stimulated vertical area versus fracture time is plotted. For these cases it was found that the dilatancy effects do not play primary role in the fracture growth. Similar results were obtained for several dilatancy angles proposed ($0°$, $10°$, $20°$, $30°$). However, limestone mechanical properties did have primary role on fracture growth, refer to Table 2. In case 0 and 1 (see Fig. 3), the vertical fracture grows beyond the mid WI plane (see Fig. 3), which means that no secondary area is being stimulated. For case 0, the limestone barrier and shale have the same mechanical properties. On the other hand, for case 1, weak barrier is adopted, mechanical properties were described in Table 2.

For case 3 (dashed red in Fig. 4), fracture growth is bounded by the barriers, which means that arrest occurs, defined in Blanton [2]. The same phenomena take place for cases 4 and 5. This mechanism leads to a longer stimulated primary fracture area, but the total stimulated area is minor in comparison with cases 0 and 1. This explanation is illustrated in Fig. 3. These results are in agreement with the mechanical properties of the barriers, where the limestone is stiffer, the primary fracture growths in length and the fracture height is limited by the distance between the horizontal barriers. For case 0 the opposite occurs, the primary fracture growths beyond the WI plane, which results in a higher vertical fracture than the one for case number 3. However, for case number 0 it reaches an smaller length. All these comments are detailed in Fig. 3.

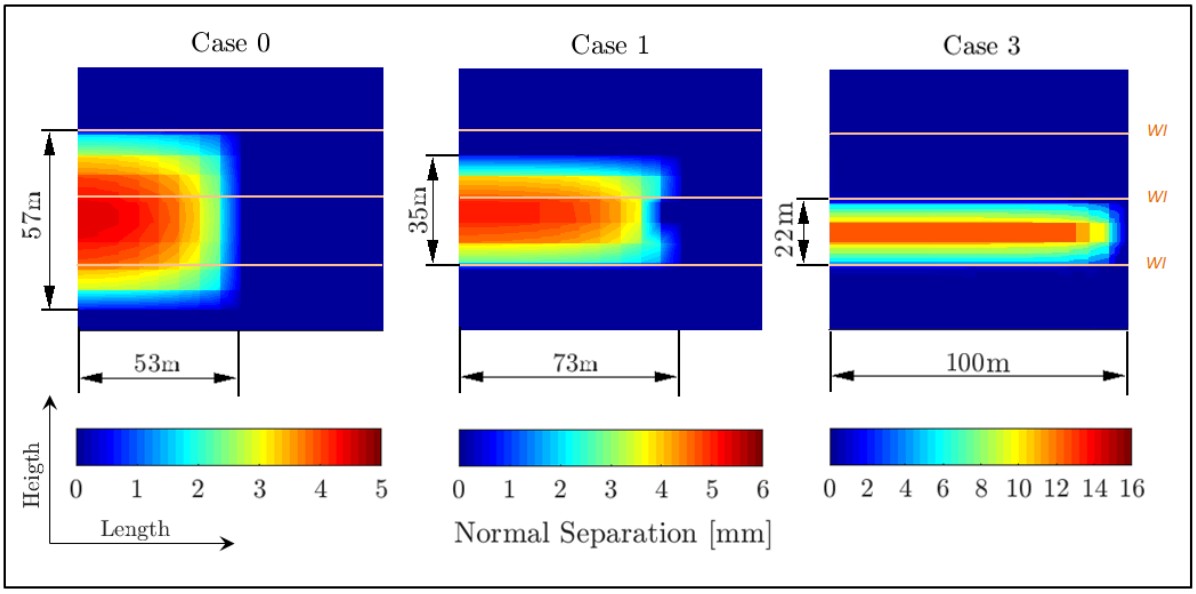

Figure 3. Vertical fracture view for each case.

As stated above the difference for each case resides on barrier properties. If the Young's modulus of the limestone barrier is smaller value (case 0 and 1), a larger stimulated vertical fracture size is obtained. On the other hand, for cases 3 and 4, the fracture is bounded by the limestone barriers. These results are represented in Fig. 4. The difference between minimal horizontal stress on limestone barriers for each case is an important component to understand (explain) these results. Hence, the fracture for case 0, is more convenient in terms of productivity. As the fracture length is reached due to limestone barriers boundary, an important conclusion can be drawn, which is the relevance of the distance between barriers. As for all these cases no horizontal fracture activation by shear stresses was observed. There is not enough contrast between shale and limestone mechanical properties to promote significant tangential displacements in the weak interface plane.

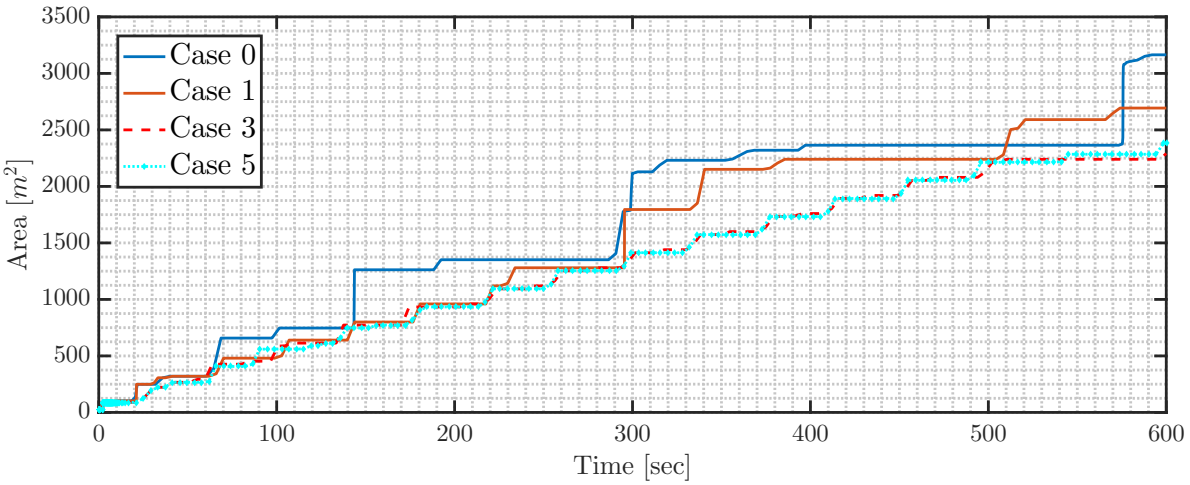

Figure 4. Primary stimulated area of fracture.

4.2 Dilatancy sensitivity

As seen in previous section, dilatancy has no effect and hence no horizontal fracture propagation. When significant contrast is found between limestone and shale stresses there is horizontal fracture propagation, see case 5. The properties of the model are given in Table 2 and the TSTR of the WI, detailed in Table 3, is halved. Finally, the angle of dilatancy is 30° for this analysis.

It can be seen in Fig. 5 that the primary fracture area does not grow once the fluid comes to stimulate the horizontal fracture. In other words, when the mechanical properties in the shale and limestone formation differ and dilatancy angle reaches the max value (30°), horizontal fracture propagation occurs. It is important to remark that this phenomena derives in a tshape fracture and takes place in a strike slip fault regime.

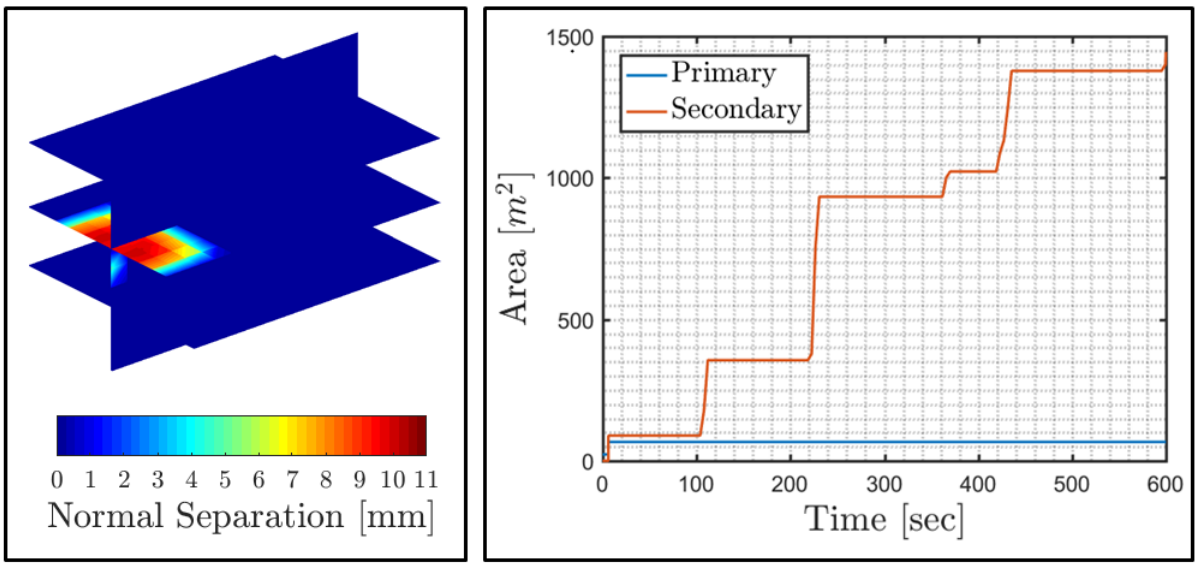

Figure 5. Left: Fracture view. Right: Primary and secondary stimulated area of fracture.

5 Conclusions

A finite element model is developed to simulate hydraulic fracture growth in a general case in order to analyse the interaction between a vertical hydraulic fracture with a weak interface horizontal plane. This paper gives a new perspective on the incidence of the dilatancy effects on the fracturing process when a strike-slip fault regime is represented and reinforces how this mechanism enhances the permeability in the weak interface planes, promoting horizontal fractures by shear stress. Moreover, this research tackles the influence of the mechanical properties in limestone barriers and studies the appearance of each mechanism (arrest, t-shapes and cross). Results will provide meaningful information to achieve a better operating window to carry out the fracture process. Together these two factors, dilatancy and barrier properties become more noticeable when the contrast of properties between layers increases. In this paper, a significant sensitivity can be observed when the E_h between layers has a relationship of 3.50 times, presenting horizontal stimulation. Otherwise, when the contrast of these properties is low, horizontal stimulation is not obtained and dilatancy has not critical effects.

In future works other features can be studied, such as: pump rates, injection points and incidence angles between the primary fracture and WI. Better understanding is needed on the WI properties to address dilatancy implications.

References

[1] Sosa and Frydman. Caracterización geomecánica de laboratorio aplicado a la formación de vaca muerta. *10° Congreso de exploración y desarrollos de hidrocarburos*, pp. 21–45, 2018.
[2] Blanton. An experimental study of interaction between hydraulically induced and pre-existing fractures. *SPE-DOE*, pp. 16–18, 1982.
[3] Celleri. Hydraulic fracture propagation in strike-slip regime with weak interfaces. *ARMA - American rock mechanics association*, pp. 21–45, 2019.
[4] Khristianovic and Zheltov. Formation of vertical fractures by means of highly viscous liquid. *Proceedings of the fourth world petroleum congress*, pp. 579–86, 1955.
[5] Perkins and Kern. Propagation of a vertical hydraulic fracture. *SPE J.*, vol. 12, n. 8, pp. 306–14, 1955.
[6] Adachi. Computer simulation of hydraulic fractures. *Int. Journal Rock Mech and Min. Sciences*, vol. 44, n. 5, pp. 739–757, 2007.
[7] Weng. Modeling of complex hydraulic fractures in naturally fractured formation. *Journal of Unconventional Oil and Gas Resources*, vol. 9, pp. 114–135, 2014.
[8] Nguyen. Modeling hydraulic fractures in porous media using flow cohesive interface elements. *Elsevier, Engineering geology*, vol. 9, pp. 68–82, 2017.
[9] Serebrinsky. Finite elements simulations of the interaction of a hydraulic fracture with a natural fracture. *ARMA - American rock mechanics association*, 2017.
[10] Frydman. Iniciação e propagação de fraturas em poços de petróleo. *PhD thesis*, 1996.
[11] Daneshy. Factors controlling the vertical growth of hydraulic fractures. *SPE Hydraulic fracturing technology conference*, 2009.
[12] Chuprakov. Hydraulic fracture height containment by weak horizontal interfaces. *SPE-173337-MS*, 2015.
[13] Detournay. Fundamentals of poroelasticity. *Comprehensive Rock Engineering*, vol. 2, pp. 113–171, 1993.
[14] de R. Borst. *Computational methods for fracture in poroues media*. Elsevier, Radawerg 29, PO Box 211, 2018.
[15] Medina et al. Numerical modeling of hydraulic fracture propagation in tectonically stressed shale reservoirs. *URTEC Unconventional Resources Technology Conference*, 2020.
[16] Scheider. Cohesive model for crack propagation analysis of structures with elastic-plastic material behaviour. *GKSS research center Geesthacht*, 2001.
[17] Frydman et al. Comprehensive determination of the far-field earth stresses for rocks with anisotropy in tectonic environment. *Society of Petroleum Engineers*, 2016.
[18] Varela and Hasbani. A rock mechanics laboratory characterization of vaca muerta formation. *American Rock Mechanics Association*, 2017.
[19] Sosa Massaro. Regional geomechanical study of the vaca muerta formation and its application to unconventional shale oil / gas reservoirs. *PhD thesis*, 2019.
[20] Hiroki Sone and Mark D. Zoback. Mechanical properties of shale gas reservoir rocks. part 1: Static and dynamic elastic properties and anisotropy. *GFZ - German Research Centre for Geosciences*, 2013.